

A Neurosymbolic Framework for Interpretable Cognitive Attack Detection in Augmented Reality

Rongqian Chen¹, Allison Andreyev¹, Yanming Xiu²,
Mahdi Imani³, Bin Li⁴, Maria Gorlatova²,
Gary Tan⁴, Tian Lan¹

¹The George Washington University, USA

²Duke University, USA

³Northeastern University, USA

⁴The Pennsylvania State University, USA

Abstract

Augmented Reality (AR) enriches perception by overlaying virtual elements on the physical world. Due to its growing popularity, cognitive attacks that alter AR content to manipulate users' semantic perception have received increasing attention. Existing detection methods often focus on visual changes, which are restricted to pixel- or image-level processing and lack semantic reasoning capabilities, or they rely on pre-trained vision-language models (VLMs), which function as black-box approaches with limited interpretability. In this paper, we present CADAR, a novel neurosymbolic approach for cognitive attack detection in AR. It fuses multimodal vision-language inputs using neural VLMs to obtain a symbolic perception-graph representation, incorporating prior knowledge, salience weighting, and temporal correlations. The model then enables particle-filter based statistical reasoning—a sequential Monte Carlo method—to detect cognitive attacks. Thus, CADAR inherits the adaptability of pre-trained VLM and the interpretability and reasoning rigor of particle filtering. Experiments on an extended AR cognitive attack dataset show accuracy improvements of up to 10.7% over strong baselines on challenging AR attack scenarios, underscoring the promise of neurosymbolic methods for effective and interpretable cognitive attack detection.

1 Introduction

Augmented Reality (AR) and Mixed Reality (MR) technologies have rapidly advanced in recent years, offering users an immersive perceptual experience by overlaying contextually relevant information and virtual objects onto their physical environment (Zheng and Yuan 2023). As AR/MR are rapidly changing how users perceive, interpret, and interact with the world around them, new vulnerabilities have emerged and attracted increasing research attention. In particular, the reliance on visual and spatial cues in AR/MR creates an implicit trust in the accuracy and authenticity of overlaid content. This trust can be exploited by adversaries to launch cognitive attacks, which use malicious manipulations of virtual content to mislead, distract, or coerce users without their awareness (Xiu, Scargill, and Gorlatova 2025; Cheng et al.



Figure 1: Illustrative AR/MR cognitive attacks. Top row: original scenes; bottom row: manipulated scenes. (a) Text Modification Attack. (b) Visual Modification attack. (c) Removal Attack. (d) Addition Attack.

2023; Teymourian et al. 2025). Unlike traditional cybersecurity threats that target data or system integrity, cognitive attacks in AR/MR (such as the examples shown in Fig. 1) operate at the perceptual level, manipulating users' semantic interpretation through subtle or deceptive visual alterations (Xiu and Gorlatova 2025).

Prior work on detecting such cognitive attacks often employs computer vision techniques to identify visual changes or adversarial distortions (Qiu et al. 2019; Duan et al. 2022a,b; Li et al. 2024; Acharya et al. 2022). However, these methods rely on pixel/image processing, lacking the ability to model the human perception process that not only involves prior knowledge and contextual information, but also selectively focuses on aspects of the visual field for semantical interpretation. As a result, these methods may struggle to capture smart cognitive attacks manipulating only a small number of pixels and also could suffer from false positives due to benign visual perturbations that do not affect users' semantic interpretation (Li et al. 2024). More recent studies propose pre-trained vision-language models (VLMs) (Xiu, Scargill, and Gorlatova 2025; Roy et al. 2025) to achieve semantic-level detection, by processing visual features and incorporating human-like knowledge. But the reasoning of pre-trained VLMs is a black-box approach offering limited interpretability. It is hard to leverage domain-specific knowledge or model scene/context evolutions or temporal correlations in cognitive attack detection.

In this paper, we consider cognitive attacks that aim to manipulate users' semantic perception in AR/MR. We pro-

pose *CADAR* (Cognitive Attack Detection in Augmented Reality), a neuro-symbolic approach encompassing two key components working in concert: (i) a symbolic perception-graph model, which is extracted using pre-trained neural VLM models to represent scene/context evolution at semantic-level, ; and (ii) a particle-filter model, which is commonly used in non-linear and stochastic systems. It applies a sequential Monte Carlo method to the perception graph for reasoning and detecting cognitive attacks, stabilizes inherently noisy or inconsistent VLM outputs, and mitigates errors or missed detections through probabilistic fusion. It also offers granular, flexible temporal detection: by using reference sequences, frame-wise inference localizes attacks per frame, to produce a variable number of labels when needed. Thus, the *CADAR* approach inherits the adaptability of pre-trained VLM (neural part), as well as the interpretability and reasoning rigor of particle filtering (symbolic part). It semantically interprets and models the sequential scene changes for robust cognitive attacks detection in AR/MR, overcoming limitations in existing work.

Our key contributions are as follows:

- **Neuro-symbolic modeling and reasoning.** We present a neuro-symbolic framework tailored to AR/MR cognitive attack detection. A pre-trained neural VLM generates symbolic perception graphs that stores objects, attributes, and relations for explicit, interpretable reasoning.
- **Perception graph representation.** We propose a perception graph schema that formally encodes multi-modal scene/context evolution at the perceptual level, integrating outputs from complementary modules (image and text encoders, object detection, and segmentation) for cognitive attack inference.
- **Particle-filter-based statistical reasoning.** We are the first to apply particle filtering to symbolic perception graphs. Not only does our method improve the robustness of stochastic VLM outputs, mitigating noise and hallucination, but it also enables interpretable statistical procedures to reason about cognitive attacks.
- **We create the Extended AR-VIM dataset,** which is the first publicly available AR cognitive attack dataset, by expanding the existing AR-VIM dataset (Xiu and Gorlatova 2025). *CADAR* evaluation shows it significantly outperforms several baselines, achieving an overall accuracy of 80.1% compared to 69.4% for the next-best model.

The rest of the paper is organized as follows: Section 2 reviews related work; Section 3 presents our method; Section 4 reports experimental results and Section 5 concludes the paper.

2 Related Work

Cognitive Attacks in AR/MR. One well-studied category of visual attacks is adversarial attacks, which introduce imperceptible yet malicious perturbations to input data to mislead machine learning models (Zhang et al. 2024a; Mumcu and Yilmaz 2024). In contrast, cognitive attacks target perception-level semantics and aim to alter a human user’s understanding of a scene (Cheng et al. 2023; Xiu and

Gorlatova 2025). Augmented Reality (AR) systems, which overlay virtual content onto the physical world to enhance perception and decision-making, are particularly vulnerable to such attacks. However, research on cognitive attacks in AR remains limited. Existing methods often rely on access to the original, unaltered scene for comparison or employ pre-trained VLMs with limited interpretability.

Knowledge Graphs. Graph-based representations offer a compact and expressive way to encode entities and the possibly complex relations among them, making graphs well-suited for downstream prediction and retrieval tasks. A knowledge graph represents each entity as a node and each semantic relation as an edge, thereby capturing structured world knowledge at scale (Hogan et al. 2021). A scene graph extends this idea to visual understanding: it organizes objects, their attributes, and inter-object relationships into a graph that supports higher-level reasoning over images and videos (Chang et al. 2021). Numerous task-specific graph formulations have also emerged, for example, mission-specific knowledge graphs for situational awareness (Yun et al. 2025), topological graphs for robot navigation (Shah et al. 2022), and interaction networks that model physical relations among objects (Battaglia et al. 2016).

Neuro-symbolic Methods. Neuro-symbolic approaches couple deep neural networks with symbolic reasoning—i.e., reasoning over explicitly represented knowledge in formal languages, to capitalize on the complementary strengths of subsymbolic pattern recognition and symbolic compositionality (Bhuyan et al. 2024). Within knowledge-graph research, most neuro-symbolic work addresses link prediction or graph completion, where the hybrid models offer interpretable rules, guided learning, and more transparent decision pathways (DeLong, Mir, and Fleuriot 2024). Yet, like standard supervised techniques, many of these solutions still demand sizable labeled datasets. In contrast, our framework introduces a neuro-symbolic reasoning module that combines explicitly encoded rules with statistics, achieving high interpretability while remaining data-efficient.

Particle Filter and Statistical Reasoning. Particle filters—sequential Monte Carlo algorithms for recursive Bayesian estimation—propagate a set of weighted samples to approximate the posterior state distribution, outperforming classical Kalman filters in strongly non-linear or non-Gaussian settings (Künsch 2013). They are widely used in surveillance, robotics, and navigation, leveraging visual, geometric, and motion cues such as color, texture, and shape (Awal et al. 2023). In *CADAR*, we model graph nodes and edges as stochastic particles, enabling robust reasoning under noisy or inconsistent VLM outputs.

3 Methodology

In this section, we define the four types of cognitive attacks in AR scenes and introduce our neuro-symbolic framework for detecting such attacks. As illustrated in Fig. 2, the framework consists of two main components: the perception graph model and the particle filter-based detection module. The

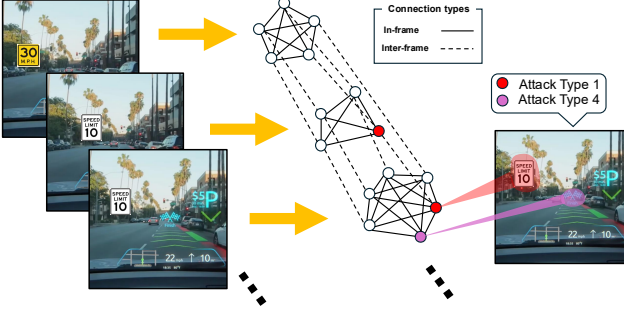


Figure 2: CADAR system overview. Sequential video frames are converted into temporal perception graphs, which the attack-detection module then analyzes to identify, classify, and localize adversarial attacks.

perception graph encodes each frame as a 3D spatiotemporal structure, where nodes represent objects and edges capture their relationships across time (Fig. 3). These structured graphs are then passed into the attack detection algorithm (Fig. 4), which reasons over the particle filter to identify cognitive attacks.

3.1 Cognitive Attacks

We study four representative adversarial attack types that compromise an AR scene’s semantics (Fig. 1).

Text-modification Attack. Altering on-scene text, e.g., overlaying “FREE PARKING” atop a “NO PARKING” sign, reverses instructions or injects false information, misleading both users and perception systems.

Visual-modification Attack. Altering an object’s appearance or position (green light to red, stop sign moved to mid-junction) distorts recognition and user judgment.

Removal Attack. Occluding or deleting safety-critical cues (e.g., an exit sign) erases vital information and breaks expected graph relations.

Addition Attack. Inserting fictitious objects or labels (e.g., a fake hazard symbol) plants misleading cues that divert attention and corrupt downstream reasoning.

3.2 Perception Graph Model

The perception graph model is a symbolic representation of perception, simulating how humans perceive, interpret, and prioritize information. It collects, structures, and stores scene data that enables formal reasoning later. The graph leverages pre-trained VLMs to approximate human interpretation of sensory input. Given AR imagery and task context, the model fuses multimodal signals into a compact graph and embeds their semantics in a latent perceptual space.

A perception graph consists of nodes and edges. Objects are represented as nodes, and object relationships are represented as edges. Given the context information and prompt (shown in the Figure 3), the VLM would extract the related objects with their relationships in the scene. At timestep t , the Perception Graph G_t is generated as follows.

Graph Construction. At discrete timestep $t \in \{1, \dots, T\}$ we ingest

$$I_t \in \mathbb{R}^{H \times W \times 3}, \quad c_t \in \mathcal{C}, \quad (1)$$

where I_t is the AR video frame and c_t encodes task context. A pre-trained vision-language module \mathcal{F}_{VLM} lifts the frame into a spatio-temporal perception graph

$$G_t = (\mathcal{V}_t, \mathcal{E}_t) = \mathcal{F}_{\text{VLM}}(I_t, c_t), \quad (2)$$

with nodes \mathcal{V}_t and edges \mathcal{E}_t :

$$\mathcal{V}_t = \{v_i^t\}_{i=1}^{N_t}, \quad \mathcal{E}_t = \{e_{ij}^t \mid v_i^t, v_j^t \in \mathcal{V}_t\}. \quad (3)$$

For reasoning that needs the *entire* observation history (e.g. long-range causal inference) we define GraphSet

$$\hat{G}_t = (\mathcal{V}_{1:t}, \mathcal{E}_{1:t}), \quad \mathcal{V}_{1:t} = \bigcup_{s=1}^t \mathcal{V}_s, \quad \mathcal{E}_{1:t} = \bigcup_{s=1}^t \mathcal{E}_s. \quad (4)$$

Thus the GraphSet \hat{G}_t is the union of all spatial and temporal connections that stitch object instances across time steps $1:t$. Each node still carries its original timestamp to preserve the temporal ordering.

Each node in the perception graph is represented by several attributes, including its ID, attack type, and timestep, along with a semantic description, visual features such as segmentation masks, a recognition probability score, contextual importance based on task relevance, and a reasonability score ranging from -3 to $+3$. These attributes are encoded using pre-trained vision-language and segmentation models to capture multimodal object representations. Each edge connects two nodes and includes similar parameters (node IDs, attack type, and timestep), along with a textual description capturing semantic, functional, navigational, or instructional relationships. Edge importance is derived from the contextual salience of the connected nodes.

NodeSet and EdgeSet. After defining the temporal graph structure \hat{G}_t , which links perception graphs across time, we introduce the NodeSet and EdgeSet to represent the temporally connected nodes and edges, respectively.

At each time step t , the NodeSet for object i is denoted as $\mathcal{N}_{i,t}$, and the collection of all such NodeSets is represented as the NodeSet List \mathcal{N}_t .

$$\mathcal{N}_{i,t} = \{v_i^k \mid 1 \leq k \leq t\}, \quad i \in \mathcal{I}_t, \quad (5)$$

$$\mathcal{N}_t = \{\mathcal{N}_{i,t} \mid i \in \mathcal{I}_t\}.$$

where $\mathcal{I}_t = \bigcup_{s=1}^t \{i \mid v_i^s \in \mathcal{V}_s\}$ is the set of all object IDs observed so far.

Similarly, EdgeSet and EdgeSet List is defined as:

$$E_{ij,t} = \{e_{ij}^k \mid 1 \leq k \leq t\}, \quad i, j \in \mathcal{I}_t, \quad (6)$$

$$E_t = \{E_{ij,t} \mid i, j \in \mathcal{I}_t\}.$$

Thus the GraphSet \hat{G}_t can also be represented by NodeSet and EdgeSet:

$$\hat{G}_t = (\mathcal{V}_{1:t}, \mathcal{E}_{1:t}), \quad \mathcal{V}_{1:t} = \bigcup_{i \in \mathcal{I}_t} \mathcal{N}_{i,t}, \quad \mathcal{E}_{1:t} = \bigcup_{i,j \in \mathcal{I}_t} E_{ij,t}. \quad (7)$$

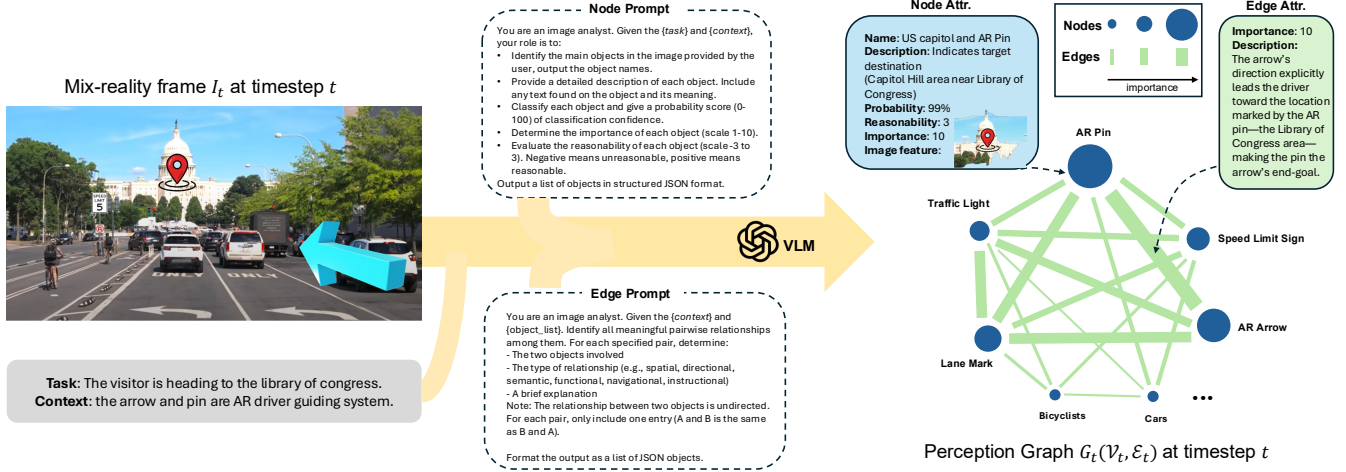


Figure 3: Perception Graph generation: Given a video frame and its contextual description, generate the corresponding perception graph at time step t .

3.3 Particle Filter Model

Our particle filter model tracks graph evolution and analyzes adversarial perturbations. It proceeds in three stages: prediction and matching, attack detection, and state estimation (cf. Fig. 4). Each entity (node or edge) is treated as a particle. At each timestep, particles match the incoming observations with prior particles. The attack detection algorithm applies statistical tests to newly matched particles and discards those marked as attacked. Finally, weighting, resampling, and estimation produces an updated, temporally consistent graph state, preserving persistent NodeSet/EdgeSet identities and the relational structure over time.

Prediction and Matching. To maintain persistent object identities across frames, we equip the NodeSet with the Prediction-Matching algorithm and use it to decide whether a newly detected Node belongs to an existing object list or creates a new one.

For any node v_i^t we denote $\mathbf{n}(v) = \text{name embedding}$, $\mathbf{d}(v) = \text{description embedding}$, $\mathbf{f}(v) = \text{visual feature embedding}$, all $\in \mathbb{R}^{d_m}$. Cosine similarity for modality $m \in \{n, d, f\}$ is defined as $\text{sim}_m(u, v)$.

Let \mathcal{A}_{t-1} be the set of NodeSet IDs that are still active at time $t - 1$. Each set maintains an Active Level $A_i^t \in [0, 3]$ (initialized to 3) indicating recent presence: if unmatched at time t , $A_i^t \leftarrow \max(0, A_i^{t-1} - 1)$; if matched, $A_i^t \leftarrow \min(3, A_i^{t-1} + 1)$. When $A_i^t = 0$, the node is considered absent and ceases matching. For every active object ID $i \in \mathcal{A}_{t-1}$ and each modality $m \in \{n, d, f\}$ compute the mean and standard deviation of pairwise similarities inside the NodeSet:

$$\mu_{i,m}^{t-1} = \frac{2}{|\mathcal{N}_{i,t-1}|(|\mathcal{N}_{i,t-1}| - 1)} \sum_{\substack{p < q \\ v_i^p, v_i^q \in \mathcal{N}_{i,t-1}}} \text{sim}_m(v_i^p, v_i^q),$$

$$\sigma_{i,m}^{t-1} = \text{StdDev}\{\text{sim}_m(v_i^p, v_i^q) \mid p < q, v_i^p, v_i^q \in \mathcal{N}_{i,t-1}\}. \quad (8)$$

To match the observed node to NodeSet, given a fresh node v_j^t and a candidate NodeSet i , define

$$s_{j,i,m} = \frac{1}{|\mathcal{N}_{i,t-1}|} \sum_{v \in \mathcal{N}_{i,t-1}} \text{sim}_m(v_j^t, v), \quad m \in \{n, d, f\}. \quad (9)$$

Candidate filter ($\leq 1\text{std}$ in every modality):

$$\mathcal{C}_j = \left\{ i \in \mathcal{A}_{t-1} \mid |s_{j,i,m} - \mu_{i,m}^{t-1}| \leq \sigma_{i,m}^{t-1}, \forall m \in \{n, d, f\} \right\}. \quad (10)$$

For each remaining candidate, measure the distance

$$D_{j,i} = \sum_{m \in \{n, d, f\}} |s_{j,i,m} - \mu_{i,m}^{t-1}|. \quad (11)$$

Finally, the assignment rule:

$$\mu_t(v_{j,t}) = \begin{cases} \arg \min_{i \in \mathcal{C}_j} D_{j,i}, & \mathcal{C}_j \neq \emptyset, \\ \text{new_id}, & \mathcal{C}_j = \emptyset. \end{cases} \quad (12)$$

If $\mu_t(v_j^t)$ returns an existing ID, append v_j^t to that NodeSet and update A_i^t ; otherwise spawn a new NodeSet. Confirmed edges e_{ab}^t are then inserted into $E_{\mu_t(a)\mu_t(b),t}$ as before.

After matching, the NodeSet goes into the Attack detection process.

Attack Detection. To detect text (Type 1) and visual (Type 2) modification attacks, those that manifest as anomalies in embedding space, we employ a dedicated statistical procedure. Because the same description embeddings are later reused when assessing EdgeSets, we illustrate the method with the NodeSet case; the extension to edges is entirely analogous. A NodeSet with a fresh match in frame t is denoted $\mathcal{N}_{i,t} = \mathcal{N}_{i,t-1} \cup \{v_i^t\}$. Let $\tilde{\mathcal{N}}_{i,t-1} \subseteq \mathcal{N}_{i,t-1}$ be the subset of nodes that *have not* been flagged as attacks in earlier frames; these constitute the “clean” reference set.

For each modality $m \in \{d, f\}$ (description embedding, visual feature embedding), we use the Principal Component Analysis (PCA) to project it to a low-dimensional space,

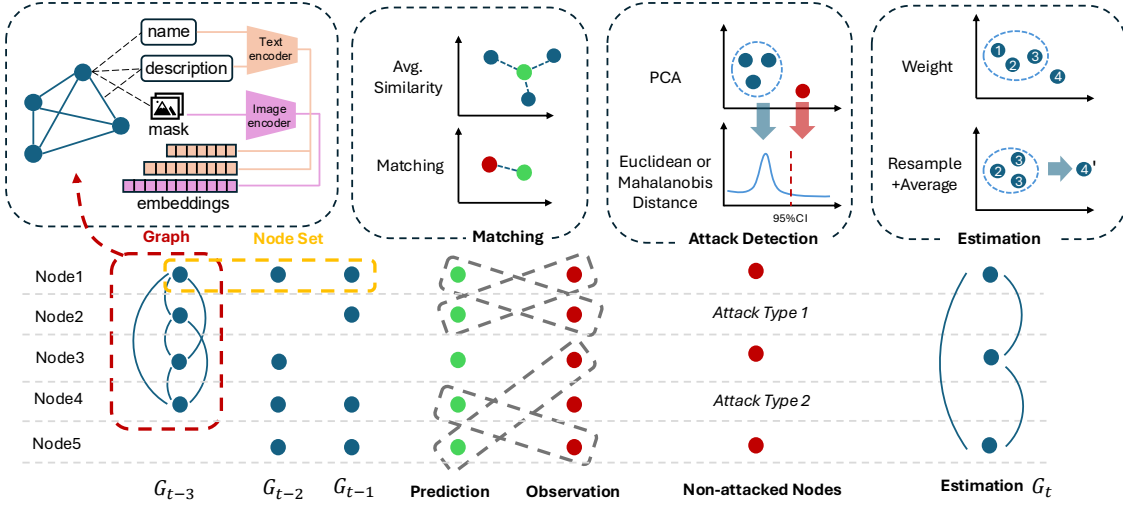


Figure 4: The particle filter-based attack detection framework consists of three main modules: matching, attack detection, and state estimation.

which removes noisy, low-variance directions. A PCA mapping on the clean reference data is computed by

$$\mathbf{W}_{i,m}^{t-1} = \text{PCA}(\{\mathbf{m}(v)\}_{v \in \tilde{\mathcal{N}}_{i,t-1}}, k_m), \quad (13)$$

where k_m is chosen such that $\geq 99\%$ variance is retained. The projected embeddings are

$$\mathbf{z}_m(v) = \mathbf{W}_{i,m}^{t-1 \top} \mathbf{m}(v) \in \mathbb{R}^{k_m}. \quad (14)$$

For each modality, fit the Gaussian reference model

$$\mathbf{z}_m(v) \sim \mathcal{N}(\mathbf{c}_{i,m}^{t-1}, \Sigma_{i,m}^{t-1}), \quad v \in \tilde{\mathcal{N}}_{i,t-1}, \quad (15)$$

with the centroid and covariance of PCA-reduced embeddings

$$\mathbf{c}_{i,m}^{t-1} = \frac{1}{|\tilde{\mathcal{N}}_{i,t-1}|} \sum_{v \in \tilde{\mathcal{N}}_{i,t-1}} \mathbf{z}_m(v), \quad (16)$$

$$\Sigma_{i,m}^{t-1} = \text{Cov}\{\mathbf{z}_m(v)\}. \quad (17)$$

Use the Mahalanobis distance for measuring Text and Visual Modification attack. For a new node v_i^t compute

$$\mathcal{M}_{i,t}^{(m)} = (\mathbf{z}_m(v_i^t) - \mathbf{c}_{i,m}^{t-1})^\top (\Sigma_{i,m}^{t-1})^{-1} (\mathbf{z}_m(v_i^t) - \mathbf{c}_{i,m}^{t-1}), \quad (18)$$

Assume under the no-attack hypothesis, the squared Mahalanobis statistic $\mathcal{M}_{i,t}^{(\cdot)} \sim \chi_{k,\alpha}^2$, which is the $(1 - \alpha)$ -quantile of a chi-square distribution with k degrees of freedom. So flag the attack as

$$v_i^t \text{ as } \begin{cases} \text{Type 1 Attack(text)} & \text{if } \mathcal{M}_{i,t}^{(d)} > \chi_{k_d,\alpha}^2, \\ \text{Type 2 Attack(image)} & \text{if } \mathcal{M}_{i,t}^{(f)} > \chi_{k_f,\alpha}^2. \end{cases} \quad (19)$$

For the structural attacks, specifically object removal (Type 3) and object addition (Type 4), the detector relies

on lightweight temporal heuristics rather than statistical distance. After each matching step the algorithm keeps a two-frame sliding window of NodeSet activity. If an object that previously carried a high task-importance score ($\pi \geq \pi_{\text{high}}$) fails to obtain a match in both the current and the immediately preceding frame, the system labels the disappearance a removal attack. Conversely, any NodeSet that first appears within the last two frames and whose reasonability score falls below a predefined threshold ($\rho \leq \rho_{\text{low}}$) is treated as an addition attack.

In the attack detection final step, if v_i^t is flagged as attack, it is appended to the $\mathcal{N}_{i,t}$ but excluded from future Gaussian updates; otherwise going to the Node Estimation process, including weight and resample, then stored in a clean reference $\tilde{\mathcal{N}}_{i,t}$.

Estimation. After a new observation $v_{i,t}$ has been matched to object i and detected as a non-attack node, the particle filter estimates the new node by refining that observation by resampling historical detections that resemble it. The estimation proceeds as follows.

Let the newly matched observation of NodeSet i at frame t be $v_{i,t}$ and denote by

$$\tilde{\mathcal{N}}_{i,t-1} = \{v^{(1)}, \dots, v^{(M)}\} \subseteq \mathcal{N}_{i,t-1}, \quad M \geq 5,$$

the set of *non-attack* detections accumulated up to $t-1$. Considering each attribute as a particle, the filter updates $v_{i,t}$ by weighted resampling over this reference set.

For any scalar attribute $a \in \{p, \pi, \rho\}$ (probability, importance, reasonability), let $a^* = a(v_i^t)$ and $a^{(j)} = a(v^{(j)})$ ($j = 1 \dots M$). Define the weight

$$\sigma_a = \max(\text{Std}\{a^{(1:M)}\}, \sigma_{\min}), \quad (20)$$

$$w_j = \frac{\exp[-(a^{(j)} - a^*)^2 / (2\sigma_a^2)]}{\sum_{k=1}^M \exp[-(a^{(k)} - a^*)^2 / (2\sigma_a^2)]}. \quad (21)$$

So w_j is the normalized weight of the particle, based on its distance to the new particle. Then use the weight to resample M indices $s_1, \dots, s_M \sim \text{Multinomial}(w_{1:M})$ yields

$$\hat{a} = \frac{1}{M} \sum_{k=1}^M a^{(s_k)}, \quad (22)$$

where \hat{a} is the estimated new scalar particle.

For embedding attributes, modality $m \in \{n, d, f\}$ (name, description, image) let $\mathbf{m}^* = \mathbf{m}(v_i^t)$ and $\mathbf{m}^{(j)} = \mathbf{m}(v^{(j)})$. Cosine similarity gives

$$\text{sim}_j = \frac{\mathbf{m}^{(j)} \cdot \mathbf{m}^*}{\|\mathbf{m}^{(j)}\| \|\mathbf{m}^*\|}, \quad w_j = \frac{\exp(\lambda_m \text{sim}_j)}{\sum_{k=1}^M \exp(\lambda_m \text{sim}_k)}, \quad (23)$$

with a scale factor $\lambda_m > 0$. Resampling as above yields indices $s_1, \dots, s_M \sim \text{Multinomial}(w_{1:M})$ and the unit-normalised mean

$$\hat{\mathbf{m}} = \frac{\sum_{k=1}^M \mathbf{m}^{(s_k)}}{\left\| \sum_{k=1}^M \mathbf{m}^{(s_k)} \right\|}, \quad (24)$$

would be the resampled embedding particle.

Finally, replacing each raw attribute in v_i^t by its resampled estimate gives the estimated node

$$\hat{v}_{i,t} = (\hat{p}, \hat{\pi}, \hat{\rho}, \hat{\mathbf{n}}, \hat{\mathbf{d}}, \hat{\mathbf{f}}), \quad (25)$$

which becomes the particle filter’s estimation state for object i at time t . If $M < 5$ (insufficient history) we skip resampling and simply set $\hat{v}_{i,t} = v_{i,t}$.

4 Experiment

In this section, we provide a detailed description of the *CADAR* implementation and the experimental settings used for our evaluation. We then present and analyze the numerical results of our experiments, demonstrating that *CADAR* significantly outperforms several baselines, achieving an overall accuracy of 80.1% compared to 69.4% for the next-best model. An ablation study is also conducted to analyze the contributions of our key components.

4.1 Implementation of CADAR

CADAR is implemented using a modular architecture. The perception graph is constructed and managed through several key components. The `Node.py` and `Edge.py` modules generate multimodal object representations by combining textual and visual features: *GPT-4.1* is used for generating descriptive text, *google/owlv2-base-patch16-ensemble* (Minderer, Gritsenko, and Hounsby 2024) enables zero-shot object detection, and *SAM2* (Ravi et al. 2024) provides object segmentation. Embeddings are extracted using *all-MiniLM-L6-v2* for object names, *all-mpnet-base-v2* for descriptions, and *ResNet-34* for image features. The `Graph.py` module manages the perception graph structure, maintaining node–edge relationships and temporal information. Temporal reasoning is handled by `NodeSet.py` and

`EdgeSet.py`, which update the graph across frames, detect potential attacks, and evolve the graph state. Attack detection is based on statistical anomaly detection using PCA to preserve 99% of variance, with thresholds computed from a 99% confidence level of the chi-squared distribution. Finally, `Utils.py` provides supporting tools for video processing and mathematical computations.

4.2 Experimental Settings

Extended AR-VIM Dataset. We base our experiments on an extended version of the AR-VIM dataset, which is specifically designed to evaluate visual information manipulation in AR environments (Xiu and Gorlatova 2025). The Extended AR-VIM is the first publicly available AR cognitive attack dataset (details in Appendix). Each sample in the dataset consists of a short video collected by an AR device (Meta Quest 3 and Samsung Galaxy S24), approximately 5-10 seconds in length, where virtual content appears at a specific frame to trigger an attack. The dataset has 160 videos in different scenes, spanning all four cognitive-attack classes. The scene covers transportation (e.g., highway, train, aircraft), experimental settings (e.g., lab equipment), industrial environments (e.g., construction, agriculture), workspaces (e.g., warehouse, office), as well as medical, daily-life, and public-safety domains. These range from altering freeway exit-ramp signage to suppressing voltage warnings on live equipment. Together, these videos provide a diverse, realistic, and tightly controlled test bed for evaluating the perception-level of cognitive attacks in AR environments. The extended AR-VIM dataset consists of 41 removal attack samples, 35 addition attack samples, 40 text manipulation attack samples, 30 visual manipulation attack samples, and 14 mix-class attack (text + visual manipulation attacks and addition + removal attacks) samples. For baseline training models, it also contains 40 non-attacked videos.

Considering the scene availability, the dataset was collected using two complementary methods: (1) The monitor-based method places AR content on a monitor screen with background images and captures it via video recording, allowing rapid and controlled generation of attack instances; (2) The real-world-based method, in contrast, uses AR headsets to capture first-person views in physical environments, introducing natural visual noise and depth information. Employing both methods is critical to capturing the trade-off between efficient data generation and real-world fidelity.

Task and Metrics. We evaluate our model on the task of attack classification in videos. *CADAR* supports frame-wise detection, variable-length multi-label outputs, and localization of multiple simultaneous attacks, which are capabilities that few existing models possess. As most baselines can only classify attacks at the video level and lack the capability for fine-grained, frame-level detection or localization, we compare *CADAR* against both advanced reasoning VLMs (*GPT-o3* and *Google Gemini 2.5* (Comanici et al. 2025)) and trained video classification models, including *3D-ResNet* (Tran et al. 2018) and *ViViT* (Arnab et al. 2021). We use accuracy and F1-score to evaluate attack detection performance: frame-wise for *CADAR*, and video-level for

Table 1: Results of the state-of-the-art methods and **CADAR** on Extended AR-VIM Dataset

Method	Attack Detection: Accuracy/F1-score (%)							Localization Acc. of attack(%)
	Text	Visual	Removal	Addition	Text+Visual	Add.+Rem.	Overall	
CADAR (Ours)	80.2/ 74.9	82.3/ 76.1	83.0/ 86.3	82.1/ 83.6	67.0/ 69.7	86.1/ 75.2	80.1/77.6	68.0
GPT-o3	62.5/56.6	23.8/29.4	76.2/66.7	61.9/55.3	16.7/25.0	14.3/25.0	39.2/39.8	-
Gemini 2.5	66.7/71.8	66.7/77.8	81.0/69.4	90.5/88.4	14.3/18.1	71.4/71.4	69.4/71.1	-
3D ResNet	12.5/22.2	57.1/72.7	57.1/34.7	42.8/31.6	-	-	42.4/40.3	-
ViViT	50.0/44.4	28.6/33.3	71.4/47.6	14.3/20.0	-	-	41.1/36.3	-

the baselines. Additionally, we report attack localization accuracy, which measures how precisely the model locates the attacks in the frame. Results are summarized in Table 1. For mixed-attack instances, a detection is considered correct only if both attack types are correctly identified.

4.3 Numerical Results and discussion

Table 1 presents the evaluation results for attack classification on the extended AR-VIM dataset. *CADAR* outperforms both the supervised learning baselines and the pre-trained VLMs. Among the different attack types, removal and addition attacks are generally easier to detect, leading to higher accuracy compared to text and visual modifications. Specifically, *CADAR* achieves a detection accuracy of 83.0% for removal attacks and 82.1% for addition attacks, compared to 80.2% for text and 82.3% for visual attacks. Notably, *CADAR* demonstrates balanced and robust performance across all attack categories, achieving superior accuracy and F1 scores. For instance, its overall accuracy/F1 score is 80.1%/77.6%, significantly higher than the next best model, *Gemini 2.5*, which scores 69.4%/71.1%.

Supervised models such as *3D-ResNet* and *ViViT* require large-scale training data and perform poorly in zero- or few-shot scenarios. For example, *3D-ResNet* achieves an overall accuracy of 42.4%, and *ViViT* achieves 41.1%. In contrast, pre-trained VLMs leverage prior knowledge and exhibit strong reasoning abilities, but their outputs are often unstable and prone to hallucination. For example, *GPT-o3* and *Gemini 2.5* achieve overall accuracies of 39.2% and 69.4%, respectively.

CADAR offers a novel approach that addresses these limitations and achieves the best overall performance. However, it is not without shortcomings. The localization accuracy is constrained by the capabilities of the zero-shot object detection and segmentation models, which struggle in complex scenes or with unfamiliar objects. *CADAR* achieves a localization accuracy of 68.0%. Moreover, reduced performance on text attacks suggests that highly subtle edits, e.g., a single-character change that scarcely alters semantics or appearance, remain difficult for the detector.

4.4 Ablation Study

Estimation Module. Fig. 5(a) shows our ablation study examining the impact of the estimation module in particle filtering. When a polluted node that might have bad data due to VLM unstable output or due to an undetected attack, the estimation module’s weighting and resampling can effectively prevent it from corrupting the ground truth knowl-

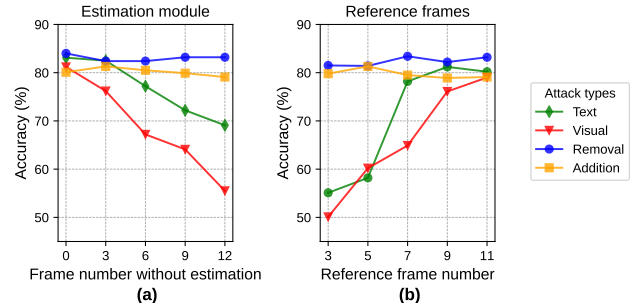


Figure 5: Ablation study on estimation module and reference frames.

edge. In the ablation study, we choose 12 videos for all attack types. As shown in the left plot of the figure, for text and visual modification attacks, the detection accuracy drops significantly as the number of frames without the estimation module increases. Specifically, the accuracy for text attacks decreases from approximately 83% to 69% and from approximately 81% to 55% for visual attacks. This indicates that the estimation module is crucial for correctly identifying and mitigating errors in more subtle attack types. In contrast, for removal and addition attacks, the accuracy remains relatively stable, suggesting these attacks are more straightforward to detect and less dependent on the estimation module’s corrective capabilities.

Reference Frames. Fig. 5(b) shows the impact of the number of reference frames on detection accuracy. A larger number of reference frames, or more prior knowledge of the scene, will result in higher accuracy. For text and visual modification attacks, increasing the number of reference frames from 3 to 11 significantly improves performance. The accuracy for text attacks increases from around 55% to 80% and from around 50% to 78% for visual attacks. This demonstrates that a larger set of reference frames provides more prior knowledge for more accurate statistical reasoning, which is essential for detecting subtle text and visual changes. Similar to the estimation module study, the detection accuracy for removal and addition attacks remains largely unaffected by the number of reference frames, consistently staying above 80%. This reinforces the finding that these attacks are less sensitive to the amount of contextual information and prior knowledge.

5 Conclusion

We presented CADAR, a neuro-symbolic framework that couples a perception graph with particle-filter reasoning to yield interpretable attack detection in AR/MR. On the Extended AR-VIM dataset, CADAR performs strongly across all attack types, and ablations highlight the value of our estimation module and richer reference histories. Limitations stem from the underlying open-vocabulary detection/segmentation, and miss very fine-grained augmentations. Future work will pursue task-specific fine-tuning of perception models, and larger-scale real-world evaluations and user studies. Overall, CADAR highlights the value of neuro-symbolic design by combining the adaptability of foundation models with symbolic reasoning for a robust and interpretable AR safety mechanism.

References

- Acharya, M.; Roy, A.; Koneripalli, K.; Jha, S.; Kanan, C.; and Divakaran, A. 2022. Detecting out-of-context objects using graph context reasoning network. In *IJCAI*.
- Arnab, A.; Deghani, M.; Heigold, G.; Sun, C.; Lučić, M.; and Schmid, C. 2021. Vivit: A video vision transformer. In *Proceedings of the IEEE/CVF international conference on computer vision*, 6836–6846.
- Awal, M. A.; Refat, M. A. R.; Naznin, F.; and Islam, M. Z. 2023. A Particle Filter Based Visual Object Tracking: A Systematic Review of Current Trends and Research Challenges. *International Journal of Advanced Computer Science & Applications*, 14(11).
- Battaglia, P. W.; Pascanu, R.; Lai, M.; Rezende, D.; and Kavukcuoglu, K. 2016. Interaction Networks for Learning about Objects, Relations and Physics. [arXiv:1612.00222](https://arxiv.org/abs/1612.00222).
- Bhuyan, B. P.; Ramdane-Cherif, A.; Tomar, R.; and Singh, T. 2024. Neuro-symbolic artificial intelligence: a survey. *Neural Computing and Applications*, 36(21): 12809–12844.
- Chang, X.; Ren, P.; Xu, P.; Li, Z.; Chen, X.; and Hauptmann, A. 2021. A comprehensive survey of scene graphs: Generation and application. *IEEE Transactions on Pattern Analysis and Machine Intelligence*, 45(1): 1–26.
- Cheng, K.; Tian, J. F.; Kohno, T.; and Roesner, F. 2023. Exploring User Reactions and Mental Models Towards Perceptual Manipulation Attacks in Mixed Reality. In *32nd USENIX Security Symposium (USENIX Security 23)*, 911–928. Anaheim, CA: USENIX Association. ISBN 978-1-939133-37-3.
- Comanici, G.; Bieber, E.; Schaekermann, M.; Pasupat, I.; Sachdeva, N.; Dhillon, I.; Blistein, M.; Ram, O.; Zhang, D.; Rosen, E.; et al. 2025. Gemini 2.5: Pushing the Frontier with Advanced Reasoning, Multimodality, Long Context, and Next Generation Agentic Capabilities. [arXiv preprint arXiv:2507.06261](https://arxiv.org/abs/2507.06261).
- DeLong, L. N.; Mir, R. F.; and Fleuriot, J. D. 2024. Neurosymbolic AI for reasoning over knowledge graphs: A survey. *IEEE Transactions on Neural Networks and Learning Systems*.
- Duan, H.; Min, X.; Shen, W.; and Zhai, G. 2022a. A unified two-stage model for separating superimposed images. In *ICASSP 2022-2022 IEEE International Conference on Acoustics, Speech and Signal Processing (ICASSP)*, 2065–2069. IEEE.
- Duan, H.; Min, X.; Zhu, Y.; Zhai, G.; Yang, X.; and Le Callet, P. 2022b. Confusing image quality assessment: Toward better augmented reality experience. *IEEE Transactions on Image Processing*, 31: 7206–7221.
- Gao, M.; Zou, Y.; Zhang, Z.; Cheng, X.; and Yu, D. 2024. Cooperative Backdoor Attack in Decentralized Reinforcement Learning with Theoretical Guarantee. [arXiv preprint arXiv:2405.15245](https://arxiv.org/abs/2405.15245).
- Hogan, A.; Blomqvist, E.; Cochez, M.; d’Amato, C.; Melo, G. D.; Gutierrez, C.; Kirrane, S.; Gayo, J. E. L.; Navigli, R.; Neumaier, S.; et al. 2021. Knowledge graphs. *ACM Computing Surveys (Csur)*, 54(4): 1–37.
- Jing, G.; Zou, Y.; Zhang, Z.; Yu, D.; Dressler, F.; and Cheng, X. 2024. Byzantine fault tolerant consensus in open wireless networks via an abstract mac layer. *IEEE Transactions on Communications*.
- Künsch, H. R. 2013. Particle filters.
- Li, Y.; Xie, B.; Guo, S.; Yang, Y.; and Xiao, B. 2024. A survey of robustness and safety of 2d and 3d deep learning models against adversarial attacks. *ACM Computing Surveys*, 56(6): 1–37.
- Minderer, M.; Gritsenko, A.; and Hounsby, N. 2024. Scaling Open-Vocabulary Object Detection. [arXiv:2306.09683](https://arxiv.org/abs/2306.09683).
- Mumcu, F.; and Yilmaz, Y. 2024. Multimodal attack detection for action recognition models. In *Proceedings of the IEEE/CVF Conference on Computer Vision and Pattern Recognition*, 2967–2976.
- Qiao, J.; Zhang, Z.; Yue, S.; Yuan, Y.; Cai, Z.; Zhang, X.; Ren, J.; and Yu, D. 2024. Br-defedr: Byzantine-robust decentralized federated reinforcement learning with fast convergence and communication efficiency. In *Ieee infocom 2024-ieee conference on computer communications*, 141–150. IEEE.
- Qiu, S.; Liu, Q.; Zhou, S.; and Wu, C. 2019. Review of artificial intelligence adversarial attack and defense technologies. *Applied Sciences*, 9(5): 909.
- Ravari, A.; Jiang, G.; Zhang, Z.; Imani, M.; Thomson, R. H.; Pyke, A. A.; Bastian, N. D.; and Lan, T. 2024. Adversarial inverse learning of defense policies conditioned on human factor models. In *2024 58th Asilomar Conference on Signals, Systems, and Computers*, 188–195. IEEE.
- Ravi, N.; Gabeur, V.; Hu, Y.-T.; Hu, R.; Ryali, C.; Ma, T.; Khedr, H.; Rädle, R.; Rolland, C.; Gustafson, L.; Mintun, E.; Pan, J.; Alwala, K. V.; Carion, N.; Wu, C.-Y.; Girshick, R.; Dollár, P.; and Feichtenhofer, C. 2024. SAM 2: Segment Anything in Images and Videos. [arXiv:2408.00714](https://arxiv.org/abs/2408.00714).
- Roy, A.; Cobb, A.; Kaur, R.; Jha, S.; Bastian, N. D.; Berenbeim, A.; Thomson, R.; Cruickshank, I.; Velasquez, A.; and Jha, S. 2025. Zero-Shot Detection of Out-of-Context Objects Using Foundation Models. In *2025 IEEE/CVF Winter Conference on Applications of Computer Vision (WACV)*, 9186–9195. IEEE.

Shah, D.; Osinski, B.; Ichter, B.; and Levine, S. 2022. LM-Nav: Robotic Navigation with Large Pre-Trained Models of Language, Vision, and Action. *arXiv:2207.04429*.

Teymourian, A.; Webb, A. M.; Gharaibeh, T.; Ghildiyal, A.; and Baggili, I. 2025. SoK: Come Together—Unifying Security, Information Theory, and Cognition for a Mixed Reality Deception Attack Ontology & Analysis Framework. *arXiv preprint arXiv:2502.09763*.

Tran, D.; Wang, H.; Torresani, L.; Ray, J.; LeCun, Y.; and Paluri, M. 2018. A closer look at spatiotemporal convolutions for action recognition. In *Proceedings of the IEEE conference on Computer Vision and Pattern Recognition*, 6450–6459.

Xiu, Y.; and Gorlatova, M. 2025. Detecting Visual Information Manipulation Attacks in Augmented Reality: A Multi-modal Semantic Reasoning Approach. *arXiv:2507.20356*.

Xiu, Y.; Scargill, T.; and Gorlatova, M. 2025. ViDDAR: Vision language model-based task-detrimental content detection for augmented reality. *IEEE transactions on visualization and computer graphics*.

Yu, F. X.; Zhang, Z.; Grob, E.; Adam, G.; Coffey, S.; Bastian, N. D.; and Lan, T. ??? Look-ahead robust network optimization with generative state predictions. In *AAAI 2025 Workshop on Artificial Intelligence for Wireless Communications and Networking (AI4WCN)*.

Yun, S.; Masukawa, R.; Na, M.; and Imani, M. 2025. Missionggn: Hierarchical multimodal gnn-based weakly supervised video anomaly recognition with mission-specific knowledge graph generation. In *2025 IEEE/CVF Winter Conference on Applications of Computer Vision (WACV)*, 4736–4745. IEEE.

Zhang, C.; Zhou, L.; Xu, X.; Wu, J.; and Liu, Z. 2024a. Adversarial attacks of vision tasks in the past 10 years: A survey. *ACM Computing Surveys*.

Zhang, C.; Zou, Y.; Zhang, Z.; Yu, D.; Gómez, J. T.; Lan, T.; Dressler, F.; and Cheng, X. 2024b. Distributed age-of-information scheduling with noma via deep reinforcement learning. *IEEE Transactions on Mobile Computing*.

Zhang, Z.; Aggarwal, V.; and Lan, T. 2025. Network diffuser for placing-scheduling service function chains with inverse demonstration. In *IEEE INFOCOM 2025-IEEE Conference on Computer Communications*, 1–10. IEEE.

Zhang, Z.; Imani, M.; and Lan, T. 2024. Modeling other players with bayesian beliefs for games with incomplete information. *arXiv preprint arXiv:2405.14122*.

Zhang, Z.; Zhou, H.; Imani, M.; Lee, T.; and Lan, T. 2025. Learning to Collaborate with Unknown Agents in the Absence of Reward. In *Proceedings of the AAAI Conference on Artificial Intelligence*, volume 39, 14502–14511.

Zheng, G.; and Yuan, L. 2023. A review of QoE research progress in metaverse. *Displays*, 77: 102389.

Zou, Y.; Zhang, Z.; Zhang, C.; Zheng, Y.; Yu, D.; and Yu, J. 2024. A distributed abstract MAC layer for cooperative learning on internet of vehicles. *IEEE Transactions on Intelligent Transportation Systems*, 25(8): 8972–8983.

A Extended AR-VIM Dataset Samples

Representative sample videos for each attack class (excluding the No Attack category) is shown below. The full dataset consists of 160 videos across diverse scenes.

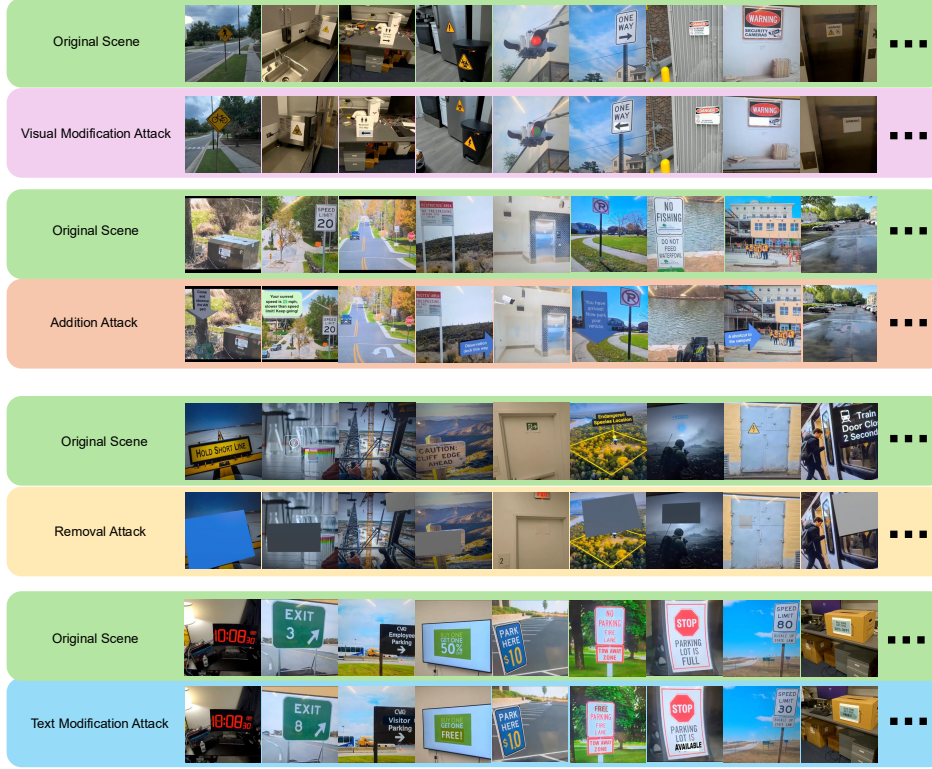


Figure 6: Sample dataset content for each AR Attack Class.

B Dataset Construction

For the real-world scenes in the Extended AR-VIM dataset, we collected additional samples using a Meta Quest 3 headset. The data collection setup is shown below

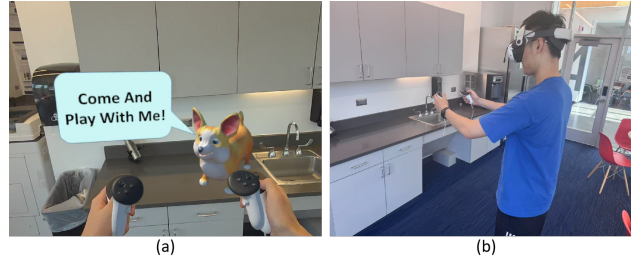


Figure 7: (a) First-person view from the AR headset: the virtual object (e.g. a dog and textual cues) is interactive and can be toggled on or off using the “Button B” on the right controller, while “Button A” starts or stops video recording. (b) Third-person view showing the data collector wearing the Meta Quest 3 headset and interacting with the AR environment using handheld controllers.

C Model Architectures and Training

For our supervised-learning baselines—ResNet and ViViT. Training hyper-parameters are shown below. We conducted all training and evaluation using Google Colab with NVIDIA A100 GPUs (40GB memory). The experiments were run in a Linux environment via Colab’s remote infrastructure, conducted using PyTorch 2.6.0 with Python 3.11.

We use ViViT-B/16x2 (pretrained on Kinetics-400) as the backbone for our ViViT model, and a 3D ResNet-18 for the ResNet baseline. Both models are trained on the full training set using inverse-frequency sampling to balance class distributions. The

	3D ResNet			ViViT		
	Value	Range	# Tried	Value	Range	# Tried
initial/end lr	5e-5	[5e-5, 5e-3]	5	1e-4	[5e-5, 5e-3]	4
weight decay	5e-3	[1e-4, 1e-1]	5	5e-3	[1e-3, 1e-1]	4
batch size	20	[8–20]	3	16	[4–16]	2
epochs	10	[5–50]	6	10	[5–50]	4
scheduler	StepLR	–	–	Cosine	–	–
optimizer	AdamW	–	–	AdamW	–	–

Table 2: Training hyper-parameters, tested ranges, and number of values tried for ViViT and 3D ResNet.

classification task involves five classes: the four attack types, along with an additional No Attack category. All input videos are resized to 400×400 pixels and normalized using a mean of [0.45, 0.45, 0.45] and a standard deviation of [0.225, 0.225, 0.225]. Each input consists of eight uniformly sampled frames from a 13-second clip. We use Focal Loss with a gamma of 2.0 as the training objective. Mixed precision (FP16) training is enabled via HuggingFace Accelerate for both models. ViViT is trained with a cosine learning rate scheduler, while the 3D ResNet uses a StepLR scheduler (step size = 10, gamma = 0.1). Final hyperparameter configurations for both models were selected based on the settings that yielded the highest validation accuracy.

D Benchmark Prompt Templates (GPT-o3 and Gemini 2.5)

For our baseline VLM models, we use the following prompt for both GPT-o3 and Google Gemini 2.5. Related work include(Zhang et al. 2025; Zou et al. 2024; Qiao et al. 2024; Zhang et al. 2024b; Jing et al. 2024; Gao et al. 2024; Ravari et al. 2024; Zhang, Aggarwal, and Lan 2025; Yu et al.; Zhang, Imani, and Lan 2024)

You are an AR video attack analyst. Your job is to identify the presence of 5 different kinds of AR attacks in the video. The definitions for each attack are as seen below: A text modification attack manipulates textual information embedded in the environment, thereby changing the semantic message conveyed by the scene. For example, replacing a NO PARKING FIRE LANE sign with one reading FREE PARKING FIRE LANE, for instance, directly reverses the intended directive and can create significant safety hazards. Such attacks are especially consequential in contexts where text offers primary contextual or navigational cues.

A visual modification attack alters an object’s appearance|its color, shape, or iconography|or repositions it in an implausible manner. Appearance changes, such as transforming a pedestrian-crossing sign into a bicycle-crossing sign or switching a green traffic signal to red, degrade recognition accuracy and mislead both human users and perception systems. Spatial changes include shifting an object away from its logical location or removing it entirely; for example, relocating a stop sign to the centre of an intersection. These manipulations can be quantified by analysing pixel-level discrepancies and deviations from expected spatial distributions.

A removal attack hides or deletes critical objects, thereby eliminating essential information and distorting scene semantics. In a fire evacuation scenario, a blank patch that obscures an emergency-exit sign on a door. By erasing this safety-critical cue, the attack deprives occupants of clear evacuation guidance, potentially endangering lives during an emergency. By analyzing nodes from the scene graph, removal attacks disrupt relational structure and semantic integrity.

An addition attack introduces new, contextually inconsistent, or misleading objects into the scene, thereby distorting its intended semantics or altering user perception. For example, a fake road sign indicating a detour is inserted into a clear street, potentially redirecting traffic and causing confusion. These attacks may include adding fictitious warning signs, virtual obstructions, or irrelevant icons that do not exist in the physical environment. Such manipulations exploit the overlay nature of AR systems and are particularly dangerous when added elements resemble legitimate cues, misleading both human users and perception models. Detection relies

on identifying unexpected objects that conflict with the scene's established structure and context.

The following input will contain a video. Please output the attack kind. Note that there may be more than 1 kind of attack present in the video, or a video could have no attack present at all. Along with the attack, mention the object the attack was performed on or describe the attack briefly in the context of the video.